WILEY

Research Article

Carbon Neutral Design of Waste Energy Recovery System for LNG Power Plant Using Organic Rankine Cycle

Minsik Choi,[1,2] **Jonghun Lim,**[1,3] **Inkyu Lee** ⓘ**,**[4,5] **and Junghwan Kim** ⓘ[3]

[1]*Green Materials and Processes R&D Group, Korea Institute of Industrial Technology, Ulsan 44413, Republic of Korea*
[2]*Department of Chemical Engineering, Konkuk University, Seoul 05029, Republic of Korea*
[3]*Department of Chemical and Biomolecular Engineering, Yonsei University, Seoul 03722, Republic of Korea*
[4]*School of Chemical Engineering, Pusan National University, Busan 46241, Republic of Korea*
[5]*Institute for Environment and Energy, Pusan National University, 2 Busandaehak-ro, 63beon-gil, Geumjeong-gu, Busan 46241, Republic of Korea*

Correspondence should be addressed to Inkyu Lee; inkyu.lee@pusan.ac.kr and Junghwan Kim; kjh24@yonsei.ac.kr

In liquefied natural gas (LNG) power plants, a significant amount of heat and cold energy is consumed to capture and store carbon dioxide (CO_2) emitted during the combustion of fossil fuels. The proposed system addresses this problem by utilizing the temperature difference between waste heat and cold energy as a power source to generate electricity. In this study, a novel waste heat and cold energy recovery system for a postcombustion LNG power plant was developed using an organic Rankine cycle (ORC). To design the proposed system, a process model was developed with the following five parts: (i) LNG vaporization, (ii) natural gas combined cycle (NGCC), (iii) amine scrubbing, (iv) CO_2 liquefaction, and (v) CO_2 injection. In the proposed system, waste LNG cold energy is used for lean amine cooling and CO_2 liquefaction. The liquefied CO_2 was pressurized to meet the injection pressure requirements. The ORC uses high-temperature exhaust gas from the NGCC as the heat source and high-pressure liquefied CO_2 as the heat sink. The economic feasibility of the proposed system was demonstrated by an economic assessment, with the net profit evaluated by a sensitivity analysis considering variations in water, electricity, and equipment costs. Consequently, the proposed system exhibited an 18.6% increase in net power production compared to the conventional system. In addition, the net profit of the proposed system exhibited a 76.7% increase compared to the conventional system, confirming its economic feasibility.

1. Introduction

As energy demand continues to rise and fossil fuels are still extensively consumed for power generation, the world faces the daunting challenge of environmental contamination due to air pollutant emissions [1]. Under these circumstances, natural gas (NG) has emerged as the fastest-growing energy resource because of its lower emissions of air pollutants [2–4]. Generally, NG is liquefied for long-distance transportation [5–7]. The transported liquefied natural gas (LNG) is then converted back to its gaseous form through LNG vaporization and burned to generate electricity in a natural gas combined cycle (NGCC) [8–10]. This process requires a significant amount of heat and cold energy [11, 12]. Cold

energy refers to a potential energy using it as the cold side of a thermodynamic cycle [13]. Therefore, the effective recovery of waste heat and cold energy from the LNG vaporization process and NGCC is crucial for reducing fuel consumption and improving overall power efficiency.

CO_2 capture and storage (CCS) requires significant heat and cold energy, and much of the energy is recovered by using the waste energy from the LNG vaporization process and NGCC [14]. In general, amine scrubbing, CO_2 liquefaction, and CO_2 injection systems are used to CCS. CO_2 is captured during the amine scrubbing process, and the captured CO_2 is liquefied during the CO_2 liquefaction process. This process requires a significant amount of energy, so waste energy from LNG power plants is used [15–17].

Nevertheless, most conventional studies have focused only on the waste heat recovery emitted from the NGCC to reduce the steam energy consumption at the regenerator in the amine scrubbing system. Ye et al. utilized an organic Rankine cycle (ORC) to recover the waste heat from reboiler condensate and employed this recovered heat in CO_2 compression processes to supply energy for a carbon capture system [18]. As a result, unit power generation increases by 0.32%, coal consumption for power generation decreases by 0.34%, cycle thermal efficiency improves by 0.23%, power generation efficiency increases by 0.15%, and the levelized cost of electricity (LCOE) decreases from 76.86 to 76.61 US$/MWh. Zhang et al. improved the energy efficiency of a monoethanolamine- (MEA-) based carbon capture plant (CCP) operating at a 95% capture rate by developing advanced process modules that make effective use of low-grade waste heat [19]. The results indicated that cascade modules exhibited remarkable energy-saving capabilities, with efficiency improvements ranging from 12.27% to 24.55%. On average, these cascade modules demonstrated a 50% enhancement compared to their single-module counterparts. Hu et al. considered an integrated system of NGCC and MEA-based CO_2 capture [20]. Waste heat was recovered using an ejector and utilized to provide heat to the reboiler. Consequently, the efficiency penalty for CO_2 capture and the power consumption were reduced by 2.67 and 4.73%, respectively. Garlapalli et al. proposed a novel heat recovery system for directly recovering waste heat in the exhaust gas for CCS [21]. Through the suggested system, the energy consumption at the regenerator reboiler can be reduced by 15.1 to 31.2%. Talebizadehsardari et al. proposed a system that uses NG as fuel; the exhaust gas from a gas turbine provides heat to run two descending cycles consisting of a steam cycle, ORC, and absorption carbon capture using MEA to extract CO_2 from the exhaust gas [22]. Ye et al. employed the ORC to recover the waste heat of a reboiler condensate and utilize the waste heat in the CO_2 compression process [18]. As a result, the thermal performance of the system and thermos-economics can be improved.

Despite the numerous contributions of conventional studies on the efficient recovery of waste heat from LNG power plants for CCS, the following challenges remain to be addressed: First, conventional studies only recover waste heat from the NGCC to reduce the power consumption of the regenerator reboiler. The cold energy is approximately 35% of the total net power requirement, so recovery of cold energy is necessary to increase the overall economic feasibility of the system. Second, a considerable amount of heat is required in the CO_2 injection system; however, conventional studies only focus on recovering waste heat to minimize power consumption at the regenerator reboiler. CO_2 injection systems also require significant heat, so it is important to minimize power consumption by utilizing waste heat.

To overcome these limitations, this study expands the system boundary beyond postcombustion NGCC to include back-side LNG regasification and front-side CO_2 liquefaction and injection. Within this expanded system boundary, this work proposed a waste heat and cold energy recovery system using an ORC. Waste heat from NGCC can be utilized for reboilers and ORC to efficiently reduce energy consumption. Additionally, by recovering the cold energy generated during LNG regasification, it is possible to maximize energy efficiency through its utilization in CCS. The aim of this approach is to overcome the limitations of conventional methods and enhance the overall power efficiency of LNG power plants for CCS, ultimately leading to reduced fuel consumption. The major contributions of this study are summarized as follows:

(1) Enhanced overall power efficiency: The overall power efficiency can be increased by recovering waste cold energy generated from the LNG vaporization process and using it in the amine scrubbing system and CO_2 liquefaction process

(2) Improved CO_2 injection system configuration: The new configuration of the CO_2 injection system using the ORC can maximize the efficiency of waste heat recovery from the NGCC, which can be utilized to pressurize and heat the liquefied CO_2. This innovative configuration leads to reduced specific net power consumption and higher power efficiency

(3) Positive environmental and economic impacts: The results showed that the proposed waste heat and cold energy recovery can increase the overall power efficiency of LNG power plants for CCS. This, in turn, translates to lower power usage, offering substantial economic and environmental benefits

2. Methodology

This section outlines a novel approach for recovering waste heat and cold energy from an LNG power plant for CCS. Figure 1 illustrates where hot and cold energy is recovered in the entire process. In Section 2.1, a brief overview of the proposed system is provided, while Section 2.2 delves into more comprehensive details and explanations of the system.

2.1. Proposed System Overview.

The simplified diagram presented in Figure 2 illustrates the proposed system's recovery of waste heat and cold energy for use in the CCS and ORC processes. The proposed system comprises the following five parts: (i) LNG vaporization, (ii) NGCC, (iii) amine scrubbing, (iv) CO_2 liquefaction, and (v) CO_2 injection using an ORC.

2.1.1. LNG Vaporization.

NG is liquefied and transported to a gas-fired power plant, where a gas/steam turbine is utilized to generate electricity [12]. However, due to the transportation and storage of LNG in cryogenic tanks, some LNG evaporates above its boiling point, creating boil-off gas (BOG) [23]. The LNG is heated by seawater through vaporization, and the compressed and recondensed BOG is converted back to gas. During the vaporization process, the released seawater contained a large amount of waste cold energy [24]. This waste cold energy is recovered during amine scrubbing and CO_2 liquefaction [25].
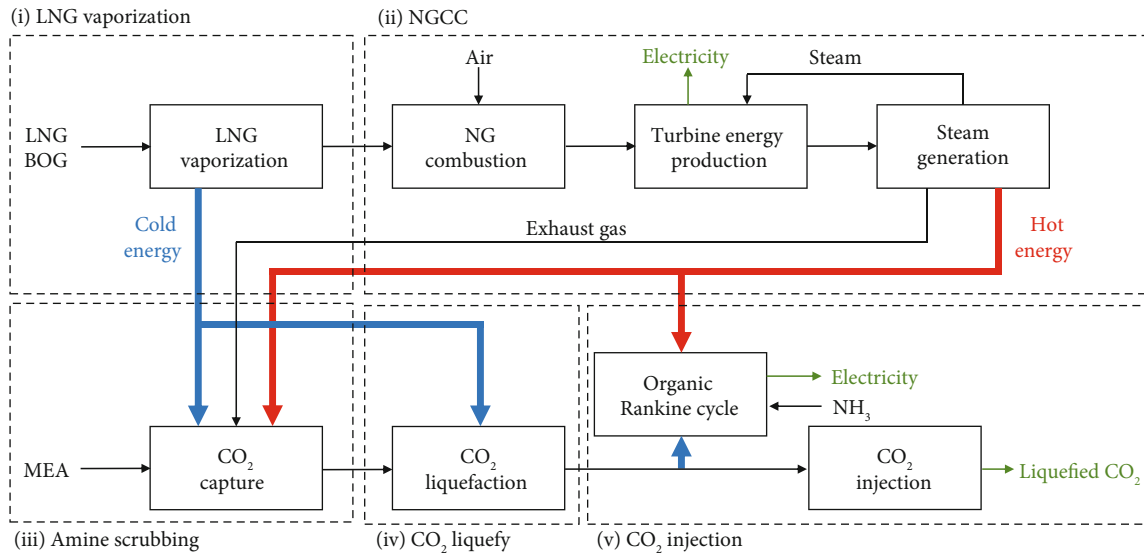
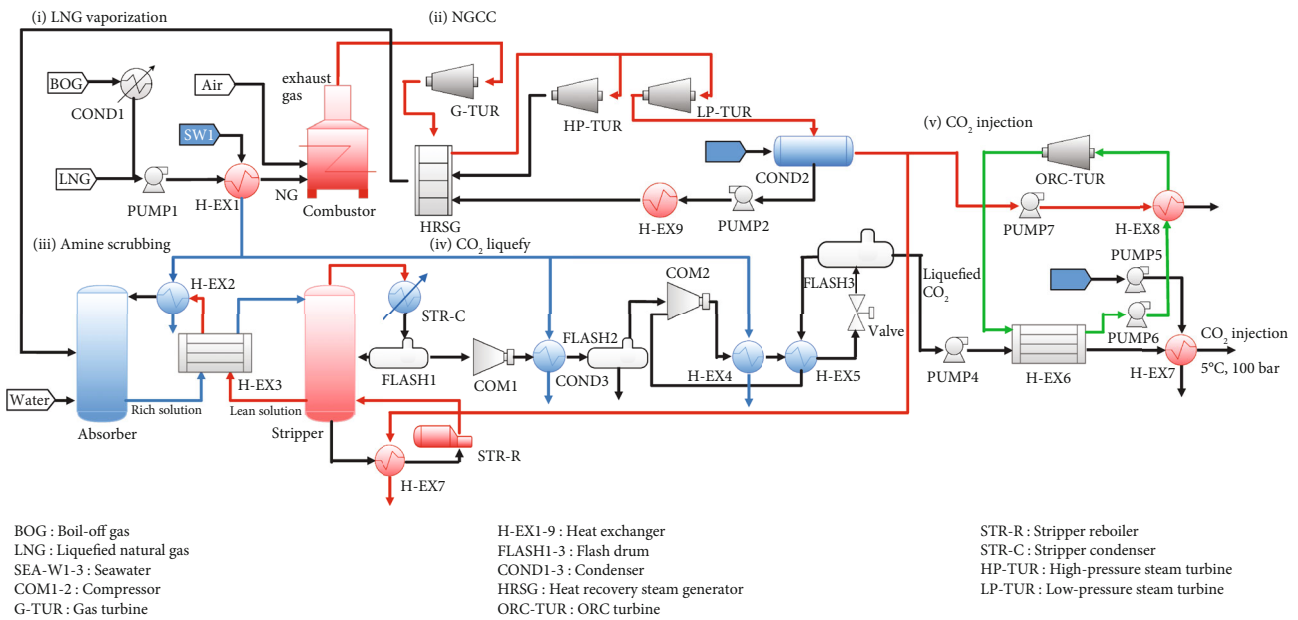Figure 1: Flowchart of the modeling simulation.

Figure 2: Simplified diagram of the suggested method for recovering wasted energy from an LNG power plant to facilitate CCS.

2.1.2. NGCC. In an NGCC combustor, regasified NG is combusted, and exhaust gas is emitted, while steam is produced in a heat recovery steam generator (HRSG) [26]. Electricity is generated by utilizing the rotational force on the output shafts of the turbines using the exhaust gas and steam. A condenser (COND2) is employed to reduce the pressure of the exhaust gases passing through the turbine and to heat the water entering the stripper reboiler (STR-R) [27]. The proposed system effectively utilizes the significant heat energy from the seawater that is discarded in conventional systems, resulting in increased energy efficiency.

2.1.3. Amine Scrubbing. To capture CO_2 generated from the exhaust gas of a combustor, amine scrubbing is commonly

used in large-scale LNG power plants. The efficiency of CO_2 capture is influenced by equilibrium constants, which vary according to the temperature and pKa difference between the amine and CO_2 [15]. The system requires a considerable amount of heat energy to regenerate the amine in the stripper reboiler (STR-R) and a substantial amount of cold energy to cool the lean amine (LEAN) solution [28]. To address this issue, the proposed system incorporates waste energy from LNG vaporization and NGCC, utilizing it to supply heat and cold energy for the STR-R and LEAN solution cooler (H-EX2), respectively.

2.1.4. CO_2 Liquefaction. The captured CO_2 undergoes liquefaction with the help of a considerable amount of cold

energy stored after the process [29]. Using the wasted cold energy from the LNG vaporization proccess, CO_2 is liquefied through a series of heat exchangers (COND3 and H-EX4).

2.1.5. CO_2 Injection. After being pressurized at the pump (PUMP4), the cold liquid CO_2 is preheated using the working fluid, ammonia (NH_3), as it passes through the heat exchanger (H-EX6) [28]. However, since the preheated CO_2 is still at a lower temperature, it undergoes further reheating using seawater. Due to the preheating of CO_2, the amount of seawater required at this point is less than that in the conventional system. ORC is a promising technology for low-temperature energy utilization [30]. The ORC is a method of producing electricity that involves four stages: (a) heat absorption, (b) expansion, (c) heat release, and (d) compression [16]. This is discussed in more detail in Section 2.2.5.

2.2. Process Model. Figure 3 illustrates the newly created design for utilizing the wasted energy from LNG vaporization and the NGCC process. The Aspen Plus V11.0 software was utilized to simulate this design, and the electrolyte-nonrandom two-liquid (NRTL) activity coefficient model was employed. The electrolyte-NRTL activity coefficient model is as follows [31]:

$$\ln \gamma_i = \frac{\sum_{j=1}^n \tau_{ji} x_j G_{ji}}{\sum_{k=1}^n x_k G_{ki}} + \sum_{j=1}^n \frac{x_j G_{ij}}{\sum_{k=1}^n x_k G_{ki}} \left(\tau_{ji} - \frac{\sum_{m=1}^n \tau_{mi} x_m G_{mi}}{\sum_{k=1}^n x_k G_{ki}} \right),$$

(1)

$$\ln \gamma_i = \ln \gamma_i^{\text{local}} + \ln \gamma_i^{\text{PDH}} = \frac{1}{RT} \left(\frac{\partial G_m^{\text{ex,local}}}{\partial n_i} \right)_{T,P,n_{j \neq i}}$$

$$+ \frac{1}{RT} \left(\frac{\partial G_m^{\text{ex,PDH}}}{\partial n_i} \right)_{T,P,n_{j \neq i}}.$$

(2)

Here, G_{ij} is the $\exp[-\tau_{ij} \alpha_{ij}]$, α_{ij} is the NRTL nonrandomness constant for the binary interaction, γ_i is the activity coefficient of component i, x_i is the mole fraction of component I, T is the temperature, m is the total number of components, τ_{ij} is the $(a_{ij} + b_{ij}T)/RT$, a_{ij} is the nontemperature-dependent energy parameter between components i and j, and b_{ij} is the temperature-dependent energy parameter between components i and j.

The design basis for each feed stream is listed in Table 1, and the reasonable assumptions are as follows:

(i) The process operates under steady-state conditions

(ii) The efficiency of the turbine and compressor was calculated to be 0.72, and the efficiency of the pump was 0.85 [14]

(iii) The pressure and temperature of seawater are fixed at 1 bar and 15°C, respectively [27]

(iv) The flow rates of steam, LNG, and exhaust gas were 5,142, 126, and 1,744 tons/h, respectively [23]

(v) Operational data from various literature sources were used to determine the specifications of each unit model involved in the LNG vaporization, NGCC, and CO_2 liquefaction parts [32–34]

(vi) The NG composition was assumed to be composed of 97% CH_4, 1% C_2H_6, 1% C_3H_8, and 1% N_2 (wt%) [35]

(vii) An open-loop system was used to model the gas/steam turbine combined cycle in an NGCC

(viii) The pressure and temperature of F-WATER (input water that is condensed in the NGCC condenser and reentered the HRSG) are set at 75 bar and 60°C, respectively [36]

(ix) One turbine model incorporates both low- and high-pressure turbines

(x) The amine-scrubbing system was assumed to have a CO_2 capture efficiency of 99% [37]

(xi) An open-loop system was used to model the ORC in the CO_2 injection part

(xii) It is assumed that there was no loss of NH_3 in the ORC [16]

2.2.1. LNG Vaporization. The NG extracted from NG production sites is subjected to liquefaction and subsequently transported to the plant as LNG. Due to the cryogenic nature of LNG, there is a possibility of evaporation above its boiling point, resulting in the formation of BOG. To utilize the BOG effectively, it undergoes recondensation in a condenser (COND1). Subsequently, a pump (PUMP1) is employed to pressurize the combined flow of LNG and BOG, increasing the pressure from 1 to 60 bar. The LNG is then heated in a heat exchanger (H-EX1) using warm seawater, thereby raising the temperature from –159 to 10°C. After the LNG is vaporized, the cooled seawater is typically discarded in the conventional system. However, in the proposed system, the waste cold energy is recovered through amine scrubbing and CO_2 liquefaction processes. To model the COND1 and PUMP1, a heater model which can determine the thermal and phase conditions of a mixture with one or more inlet streams is used, with specified outlet pressures of 1.03 and 60 bar, respectively. The outlet stream temperatures are set at –140 and –159°C, correspondingly. A HeatX model which can perform a full zone analysis with heat transfer coefficient and pressure drop estimation for single- and two-phase streams is employed as the LNG vaporizer, with its outlet temperature at 10°C [38].

2.2.2. NGCC. The NGCC power generation process utilizes steam generated by burning vaporized NG to drive a turbine and produce electricity. Compressed air and NG are combined to produce exhaust gas, which reaches temperatures of approximately 2200°C. A gas turbine is used to generate electricity by harnessing the heat in the exhaust gas. However, the exhaust gas retains high thermal energy, with a temperature of 1244°C. Consequently, a heat recovery steam
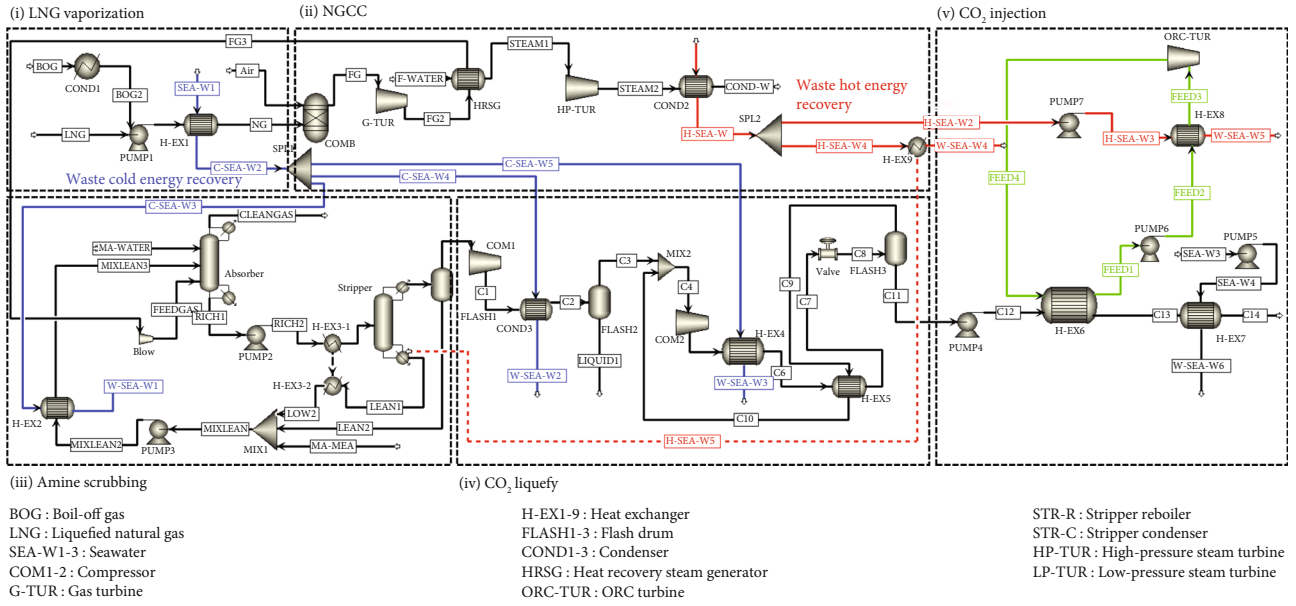
FIGURE 3: The developed model suggests utilizing wasted energy from an LNG power plant to support CCS.
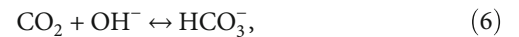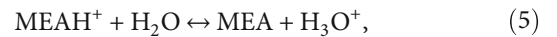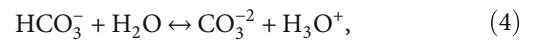
TABLE 1: Values of the feed stream.

Parameter	Feed	Values
	LNG	−162°C [38]
	BOG	−50°C [38]
Temperature	Air	20°C [17]
	MEA	38°C [37]
	NH_3	−19.7°C [16]
	LNG	1 bar [38]
	BOG	1.03 bar [38]
Pressure	Air	1 bar [17]
	MEA	1 bar [37]
	NH_3	1.9 bar [16]
	LNG	126 tons/h [23]
	BOG	0.03 tons/h [23]
Mass flow rate	Air	5,016 tons/h [23]
	MEA	0.4 tons/h [37]
	NH_3	1,653 tons/h [16]

MEA = monoethanolamine.

generator (HRSG) is employed to extract additional power by producing more steam using the excess thermal energy. The generated steam is then directed through high- and low-pressure turbines to produce electricity. To increase the pressure of the steam, a condenser (COND2) is used, which supplies heated water to the stripper reboiler. The remaining energy is utilized to heat the working fluid in the ORC at the CO_2 injection. The combustor, gas turbine, integrated steam turbine, and condenser are modeled using the RGibbs, which can also calculate the chemical equilibria between any number of conventional solid components and the fluid phases, and the Compr, which can be used to rate a

single stage of a compressor or a single wheel of a compressor, by specifying the related performance curves, heater, and HeatX models, respectively. Each component is configured with specific pressure and temperature conditions. The pressure and temperature of the combustor are given as 40 bar and 2,220°C, while the discharge pressure of the gas turbine is 1.06 bar, and that of the integrated turbine is 1.0 bar [36].

2.2.3. *Amine Scrubbing.* The CO_2 contained in the exhaust gas produced by the combined-cycle gas/steam turbine boiler was captured using an amine-scrubbing part. To accomplish this, a large-scale plant uses an amine-scrubbing system that employs MEA as a CO_2 absorbent. This part consists of an absorber that absorbs CO_2 and a stripper that regenerates CO_2. The tray columns in the absorber have bubble caps that facilitate contact between the liquid and gas. CO_2 gas is absorbed through an exothermic reaction, and the following Equations (3)–(7) describe the CO_2 absorption process [39]:

$$2H_2O \leftrightarrow H_3O^+ + OH^-, \tag{3}$$

$$HCO_3^- + H_2O \leftrightarrow CO_3^{-2} + H_3O^+, \tag{4}$$

$$MEAH^+ + H_2O \leftrightarrow MEA + H_3O^+, \tag{5}$$

$$CO_2 + OH^- \leftrightarrow HCO_3^-, \tag{6}$$

$$MEA + CO_2 + H_2O \leftrightarrow MEACOO^- + H_3O^+. \tag{7}$$

Before absorbing CO_2, the MEA solution is referred to as the LEAN solution, and after CO_2 absorption, it becomes the rich amine (RICH) solution. The transformation from LEAN to RICH occurs after absorbing CO_2 from the bubble cap, and the RICH solution is regenerated in the stripper to become LEAN again. Before entering the stripper reboiler

(STR-R), the RICH is preheated by passing it through a heat exchanger (H-EX3), thereby reducing the heat load on the STR-R. The stripper then uses steam from the reboiler to heat the amine solution and promote CO_2 recovery. At this time, the reboiler requires a considerable amount of heat; however, the efficiency is improved by utilizing the remaining heat from the NGCC. The reaction in the stripper and absorber depends on the equilibrium constant (K_{eq}), determined by the temperature. Figure 4 illustrates a simple diagram of the reaction.

When the absorber temperature is low, the difference in pKa between MEA and CO_2 is considerable, leading to a positive absorption reaction with an equilibrium constant of 1,348. Conversely, when the stripper temperature is high, the pKa difference decreases, resulting in CO_2 recovery with an equilibrium constant of 3.98. The correlation between the pKa and the equilibrium constants can be expressed by the following equation [15]:

$$K_{a,\text{acid}} = \frac{[\text{Acid}^-][\text{H}^+]}{[H\text{Acid}]}, \qquad (8)$$

$$K_{a,\text{amine}} = \frac{[\text{Amine}][\text{H}^+]}{[\text{AmineH}^+]}, \qquad (9)$$

$$\log K_{eq} = \log K_{a,\text{acid}} - \log K_{a,\text{amine}}, \qquad (10)$$

$$\log K_{eq} = \text{p}K_{a,\text{amine}} - \text{p}K_{a,\text{acid}}. \qquad (11)$$

Typically, the absorber benefits from a higher gas inlet pressure resulting from an upsurge in the CO_2 partial pressure. However, the liquid sorbent's bulk concentration may appear significant if the CO_2 is substantially depressurized or the sorbent conversion rate is elevated. Assuming that the sorbent concentration remains constant, the amine and H_2S absorption rates can be expressed using [11]

$$r = k\left(C_{H_2S} - C^*_{H_2S}\right). \qquad (12)$$

When the gas pressure increases, the gas concentration in the same volume increases. Equation (13) represents this relationship [11].

$$r = k\left(P_{H_2S} - P^*_{H_2S}\right). \qquad (13)$$

The rate constant k increases as the gas pressure increases, resulting in increased absorption efficiency at equilibrium. However, the absorption and recovery processes involve pressure changes. A high pressure of 13 bar promotes the absorption of CO_2 in the absorber. The pressure in the amine flash drum was lowered to approximately 5 bar, and the vapor was easier to remove. The pressure was then reduced to approximately 2.1 bar, allowing effective CO_2 removal from the stripper.

The exhaust gas was released as a clean gas after CO_2 was removed. The amine solution was recovered from the stripper and reused by repeating the previous process. The LEAN solution is cooled through a heat exchanger (H-EX3) and

reenters the absorber through H-EX2. However, this process consumes a large amount of heat energy during CO_2 recovery and substantial cold energy to cool the LEAN solution. To address this issue, the proposed method recovers waste energy from LNG vaporization and the NGCC. This recovered waste energy is then utilized to meet the heat and energy requirements of STR-R and H-EX2. The Radfrac model which is a rigorous model for simulating all types of multistage vapor-liquid fractionation operations was employed to simulate the performance of the stripper. The stripper has 11 stages, a 0.05 bar pressure drop in each column, a 0.5 reflux ratio, and a 0.7 boiling ratio [37].

2.2.4. CO_2 Liquefaction. This subsection discusses the liquefied CO_2 captured in the amine-scrubbing part, which requires significant energy for CO_2 cooling. The proposed method involves the utilization of the Linde-dual pressure system to liquefy CO_2. This system utilizes a cold gas stream produced by a Joule-Thomson valve to cool the incoming compressed CO_2. The CO_2 from the stripper first enters the compressor (COM1) to be compressed. The initially compressed CO_2 passing through the compressor (COM1) increases in temperature during the pressurization process; therefore, it is cooled in the condenser (COND3) by the cold energy left over from the LNG vaporization part. The liquefied CO_2 captured in the amine-scrubbing part requires additional compression and cooling because its pressure (19.7 bar) and temperature (35°C) are still too low for liquefaction. For this purpose, the initially compressed CO_2 is further compressed and cooled in a compressor (COM2) and a heat exchanger (H-EX4). The CO_2 flow (C6) with a pressure of 100 bar and a temperature of 35°C is expanded at the Joule-Thomson valve, which reduces the temperature and pressure to –96°C and 19.7 bar, respectively. A portion of this flow becomes liquid (C11), and the remainder (C9) reenters the heat exchanger (H-EX5) as a gas for cooling. The compressors (COM1 and COM2) are Aspen's Compr models, and the discharge pressures are set to 19.7 and 100 bar, respectively. The condenser (COND3) and heat exchangers (H-EX4, H-EX5) were modeled using HeatX, and the outlet temperature was set to 35°C for both [40].

2.2.5. CO_2 Injection. In this process, NH_3 was used as the working fluid. NH_3, i-butane, and propane, which are environmentally friendly and widely used, were considered as working fluids. Through a comparison of power production for each working fluid shown in Table 2, NH_3 with the highest power production was finally selected [16]. And NH_3 has a molar mass of 17 g/mol, similar to that of water (18 g/mol); thus, an existing steam turbine can be used. NH_3 without moisture is not corrosive in most materials. Since this study used pure ammonia, it is not limited by material [41]. NH_3 in the ORC preheats the liquefied CO_2 pressurized by the pump (PUMP4).

In this process, a two-phase ORC was used. ORC operating in two-phase conditions under certain temperature or working fluid conditions can result in higher efficiencies than basic ORC [42]. The ORC involves four main processes for electricity generation: (a) heat absorption, (b) expansion, (c)
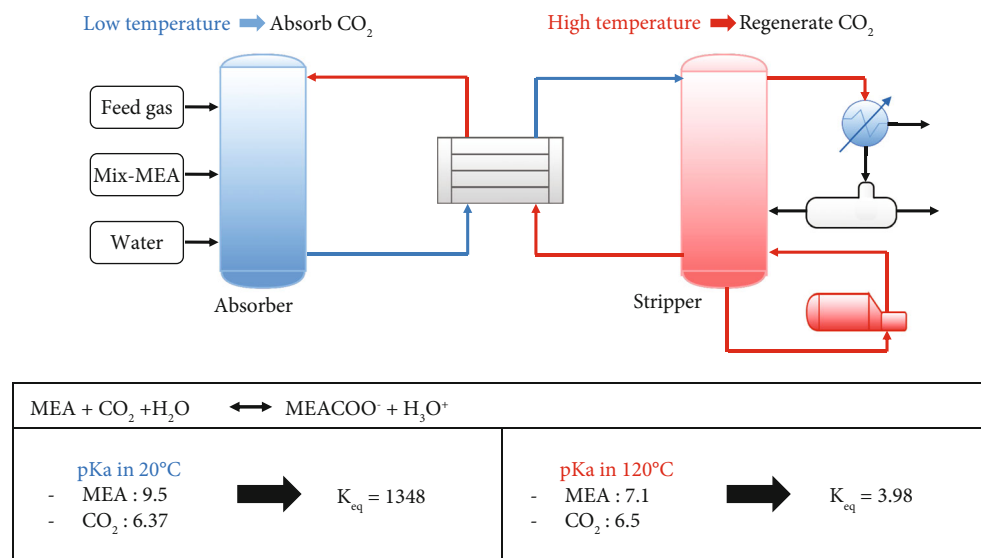
FIGURE 4: A simple process diagram of the conventional amine-based CCS process.

TABLE 2: Comparison of the working fluid.

Working fluid	Power production (kJ/kg)
NH_3 (ammonia)	121.9
C_4H_{10} (i-butane)	23.9
C_3H_8 (propane)	65.4

heat release, and (d) compression. The pressure-enthalpy diagram of NH_3 shown in Figure 5 illustrates the partially evaporated ORC process. Initially, NH_3 undergoes evaporation by absorbing heat from H-SEA-W3, after which it enters the ORC turbine (ORC-TUR) (A→B). The temperature of the NH_3 rises from –19.7 to 38°C, at which time the NH_3 is vaporized. Following evaporation, NH_3 expands at the ORC-TUR, which reduces the pressure (B→C). The expansion process produces electricity, representing the enthalpy difference between B and C. The NH_3 is cooled to –19.7°C by the cold CO_2 stream and liquefied again (C→D). Afterward, the fluid is pressurized from 1.9 bar to 6.23 bar (D→A), preparing it to repeat the entire process.

3. Results and Discussion

Finally, the waste energy from the LNG utilization process was effectively used to generate the energy required for the CO_2 capture and injection processes. An economic analysis was conducted to determine the net profit and demonstrate the economic feasibility of the proposed system. Additionally, a sensitivity analysis was performed to assess the impact of variations in water, electricity, and equipment costs on the net profit. For comparison purposes, a conventional system without waste heat utilization, combined with a CO_2 capture and injection process, was adopted as the reference structure for the LNG plant [43]. Figure 6 shows a diagram of the system.

3.1. Simulation Results. To illustrate the power efficiency of the proposed system, the overall power consumption of the conventional and proposed systems was compared. The simulation findings for both systems are listed in Table 3.

According to Table 3, the power consumption of H-EX2, COND3, and H-EX4 can be completely offset by utilizing the waste cold energy from LNG vaporization. This leads to a significant reduction in the overall cold energy requirement from 261 to 179 MW, resulting in a savings of 31% in cold energy consumption. Additionally, the power consumption of the stripper reboiler (STR-R) was reduced from 420 to 248 MW due to the utilization of the remaining energy from NGCC to heat the water entering the STR-R. This represents a saving of approximately 41% in heat energy consumption. As a result, the overall power consumption was reduced by 33% through the recovery of waste energy. Figure 7 illustrates a graph comparing the net power production between the existing and proposed systems.

According to the data presented in Figure 7, the power consumption during LNG vaporization is identical for both the conventional and proposed systems, which is 13.7 MW. However, during amine scrubbing, the power consumption of the conventional and proposed systems was 617 and 431 MW, respectively. This indicates that the proposed system could save approximately 30% of the energy consumed by the amine-scrubbing system. At CO_2 liquefaction, the power consumption of the conventional and proposed systems was 110 and 42 MW, respectively. By recovering the waste cold energy, it is possible to reduce power consumption by 61% in the liquefied CO_2 system. In terms of CO_2 injection, the proposed system consumes more power (13.7 MW) than the conventional system (1.3 MW). However, the turbine in the proposed system generated an additional 46 MW of power, which exceeds the power consumed, resulting in a net increase in power generation. Lastly, the overall power consumption of the conventional and proposed systems was 738.4 and 496.9 MW, respectively. With
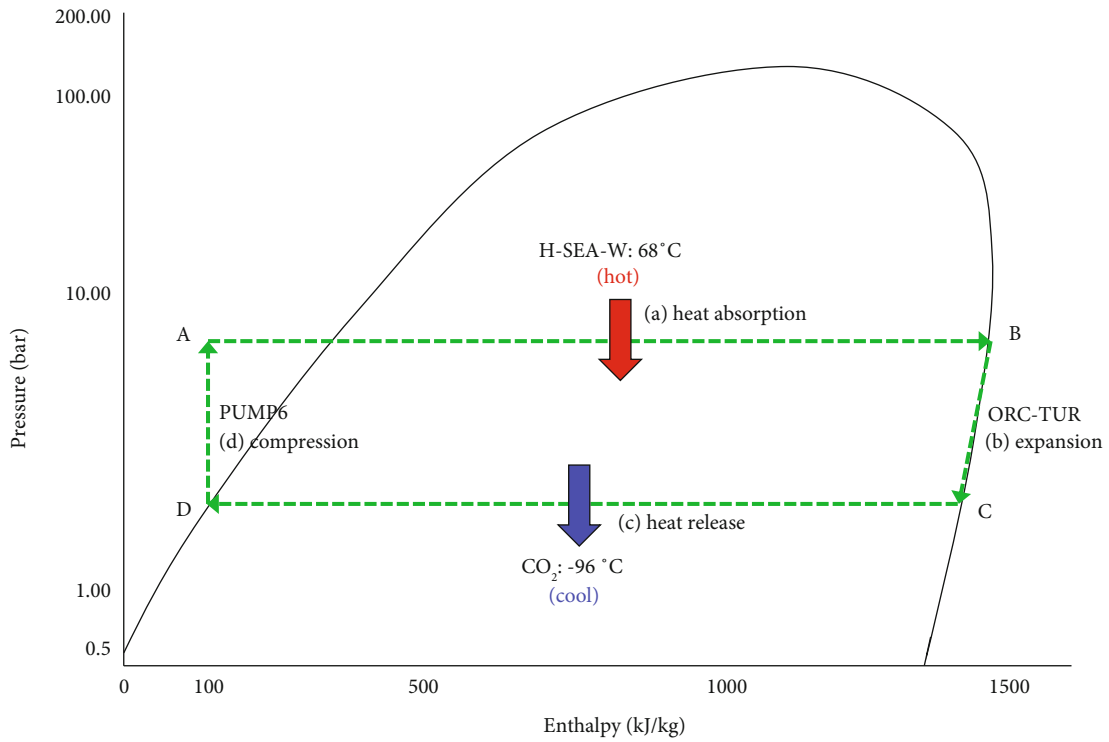
FIGURE 5: P-h diagram of the ORC.

BOG : Boil-off gas
LNG : Liquefied natural gas
SEA-W1-3 : Seawater
COM1-2 : Compressor
G-TUR : Gas turbine

H-EX1-9 : Heat exchanger
FLASH1-3 : Flash drum
COND1-3 : Condenser
HRSG : Heat recovery steam generator
S-TUR : Steam turbine

STR-R : Stripper reboiler
STR-C : Stripper condenser
HP-TUR : High-pressure steam turbine
LP-TUR : Low-pressure steam turbine
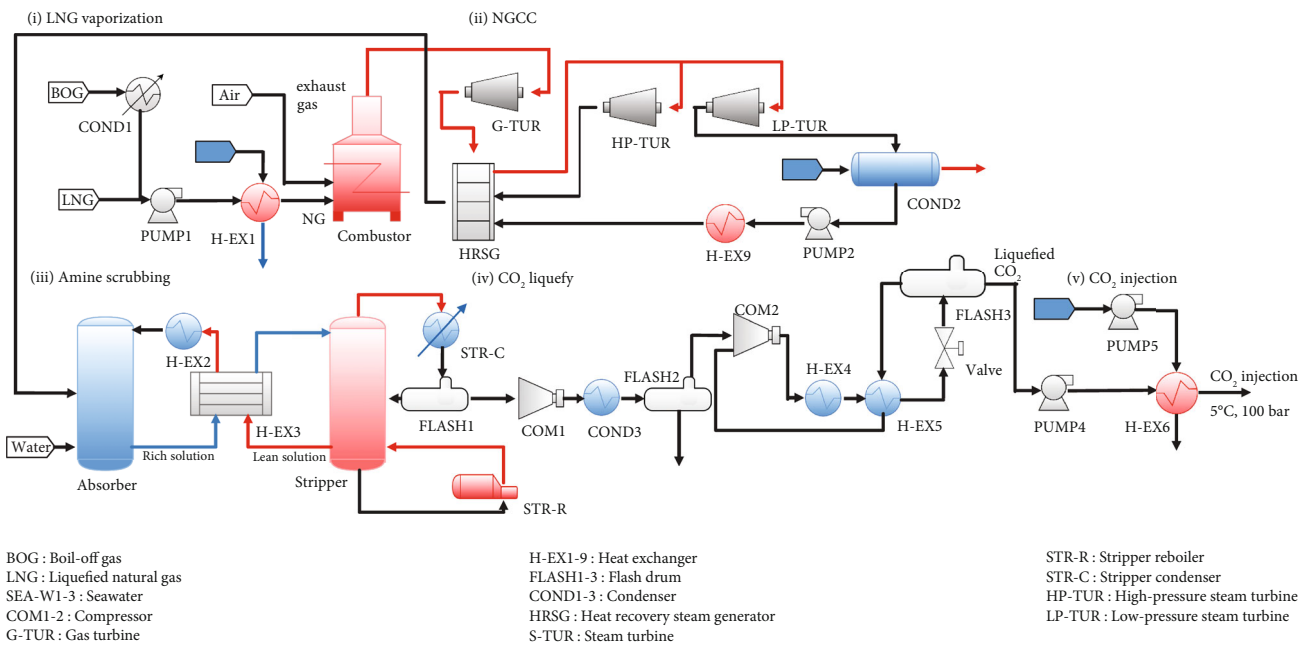
FIGURE 6: Simplified diagram of the conventional system (without heat and cold recovery).

an additional 46 MW of power over the conventional system, the total net power production was 287.5 MW, which is an increase of 18.6%. This was compared with five conventional studies to assess the enhancements in energy efficiency. Table 4 presents the contrast between the overall energy-saving rates of the proposed system and those of traditional studies.

Most traditional studies have primarily focused on reducing the amount of heat energy in reboilers. Table 4 illustrates that the proposed system displays a higher overall energy-saving ratio than other conventional methods. This is because, unlike traditional studies, the proposed system uses excess cold energy to increase the efficiency of the CCS process, resulting in the potential for higher

TABLE 3: Comparison of conventional and proposed process.

Classification		Energy consumption of conventional process	Energy consumption of proposed process	Unit
(i) LNG vaporization	COND1	1.5	1.5	kW
	PUMP1	13.7	13.7	MW
(ii) Amine scrubbing	H-EX2	13.9	0	MW
	STR-R	420	248	MW
	PUMP2	0.5	0.5	MW
	PUMP3	3.8	3.8	kW
	STR-C	179	179	MW
(iii) CO_2 liquefaction	COM1	30	30	MW
	H-EX4	33	0	MW
	COM2	12	12	MW
	COND3	35	0	MW
(iv) CO_2 injection	PUMP4	0.7	0.7	MW
	PUMP5	644	65	kW
	PUMP6	0	12	MW
	PUMP7	0	1.0	MW
Overall energy consumption		738.4	496.9	MW
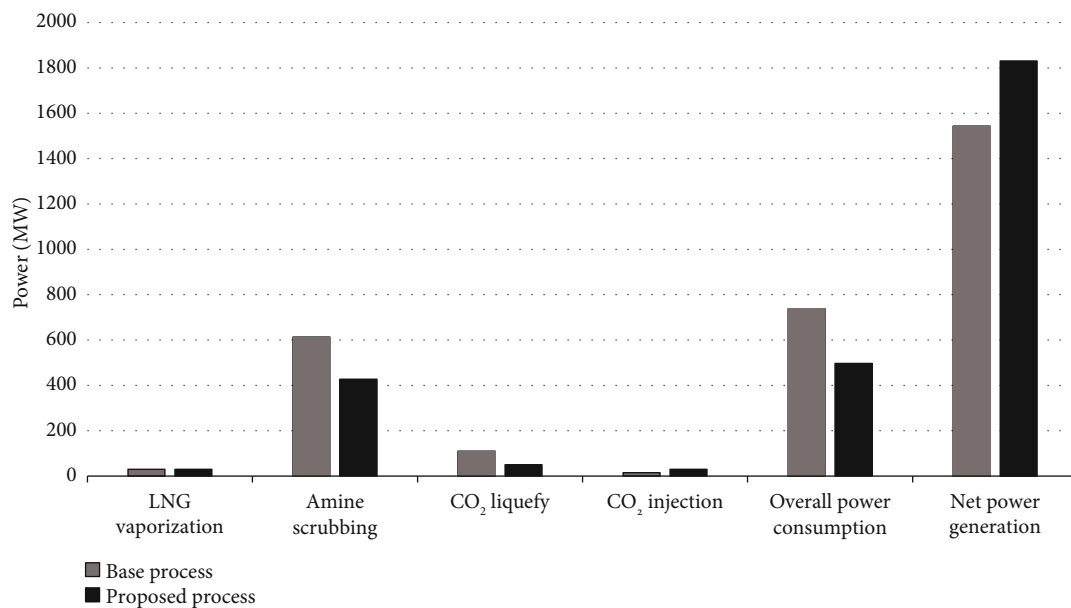
FIGURE 7: Comparison of conventional and proposed system power consumption and generation.

TABLE 4: Comparison of the overall energy-saving ratio with traditional studies and the proposed system.

Classification	Heat energy-saving ratio	Cold energy-saving ratio	Overall energy-saving ratio	Unit
Ahn et al. [44]	9–12	—	5–7	%
Duan et al. [45]	56	—	32	%
Hu et al. [20]	5	—	3	%
Garlapalli et al. [21]	15–31	—	9–18	%
Jung et al. [46]	20	—	6	%
Proposed system	41	31	33	%

TABLE 5: The overall cost of capital investment for the conventional and proposed systems.

Classification	% of FCI	Conventional (US$/y)	Proposed (US$/y)
Direct cost			
ISBL			
Piping	10	46,420,000	48,230,000
Electrical	5	23,210,000	24,115,000
Instrumentation and control	5	23,210,000	24,115,000
Equipment cost [15, 56–59]	30	139,260,000	144,690,000
Equipment installation	10	46,420,000	48,230,000
OSBL			
Land	2	9,284,000	9,646,000
Building and building services	8	37,136,000	38,584,000
Service facilities	8	37,136,000	38,584,000
Yard improvements	2	9,284,000	9,646,000
Total direct cost		371,360,000	385,840,000
Indirect cost			
Contingency	5	23,210,000	24,115,000
Contractor	5	23,210,000	24,115,000
Engineering	5	23,210,000	24,115,000
Construction	5	23,210,000	24,115,000
Total indirect cost		92,840,000	96,460,000
FCI	100	464,200,000	482,300,000
WCI	10	46,420,000	48,230,000
SUC	10	46,420,000	48,230,000
TCI		557,040,000	578,760,000
EAC ($n = 10$ yr, $r = 5\%$)		72,140,000	74,952,000

overall energy savings than other processes. Cold energy usage represents 35% of the overall energy consumption, which is a significant amount and cannot be overlooked. Notably, a study conducted by Duan et al. showed high energy efficiency by optimizing only heat energy savings [45]. Therefore, future studies should aimed at optimizing both heat and cold waste energy to further enhance energy efficiency.

3.2. Economic Analysis. In this section, all calculations were based on 2023. An economic analysis is conducted to evaluate the feasibility of the proposed system in comparison to the conventional system. The net profit is considered a key indicator to assess the viability of the proposed system. Equation (14) is used to calculate the net profit by computing the revenue (Revenue), equivalent annual cost (EAC), and total product cost (TPC) [47].

$$\text{Net profit} = \text{Revenue} - \text{EAC} - \text{TPC}. \tag{14}$$

3.2.1. Equivalent Annual Cost. EAC is the present value of the long-term, recurring upfront, and operational costs, expressed as the average cost per year. To calculate the EAC, it is necessary to determine both the annuity factor (AF) and the total capital cost (TCI). AF is a numeric quantity used to compute the current value of a sequence of uniform payments. The TCI is the sum of all the money needed to get businesses up

and running. When calculating the TCI, it is necessary to consider the initial capital investment and operating expenses such as rent, utilities, payroll, and marketing costs. Equations (15) and (16) help determine the AF and TCI, and Equation (17) for calculating the EAC [48–50].

$$\text{AF} = \frac{1 - (1/(1 + r)^n)}{r}, \tag{15}$$

$$\text{TCI} = \text{FCI} + \text{WCI} + \text{SUC}, \tag{16}$$

$$\text{EAC} = \frac{\text{TCI}}{\text{AF}}. \tag{17}$$

Fixed capital investment (FCI) is money invested in purchasing productive assets such as buildings, machinery, equipment, and distribution networks for long-term use. The FCI is calculated as the sum of the direct cost (C_{direct}) and indirect cost (C_{indirect}), as shown in [51]

$$\text{FCI} = C_{\text{direct}} + C_{\text{indirect}}. \tag{18}$$

C_{direct} is the sum of the inside battery limit cost (C_{ISBL}) and the outside battery limit cost (C_{OSBL}). C_{ISBL} comprises those directly involved in the design, construction, operation, and maintenance of the project, whereas C_{OSBL} comprises those involved outside the project, such as in fuel supply, power

Table 6: The total cost and revenue of the conventional and proposed systems.

| Classification	Range	Conventional (US$/y)	Proposed (US$/y)
Direct production cost			
Electricity [54]		423,064,200	285,269,600
Supervision labor (S)	30% of OL	63,404,000	50,124,000
Operating labor (OL)	15% of TPC	211,345,700	167,080,000
Laboratory	15% of OL	31,702,000	25,062,000
Operating supplies	15% of M	2,785,000	2,778,000
Maintenance (M)	4% of FCI	18,568,000	18,523,000
Plant overhead	60% of M + OL + S	175,990,000	141,436,000
Water [62]		236,184,000	236,184,000
Local taxes, insurance	1% of FCI	4,642,000	4,631,000
General expenses			
R&D cost	3.5% of TPC	49,314,000	39,658,700
Distribution and marketing	11% of TPC	154,987,000	124,641,600
Administrative cost	17.5% of OL	36,985,500	29,744,000
TPC		1,408,791,400	1,133,106,000
Revenue [14]		1,871,350,000	1,897,542,400
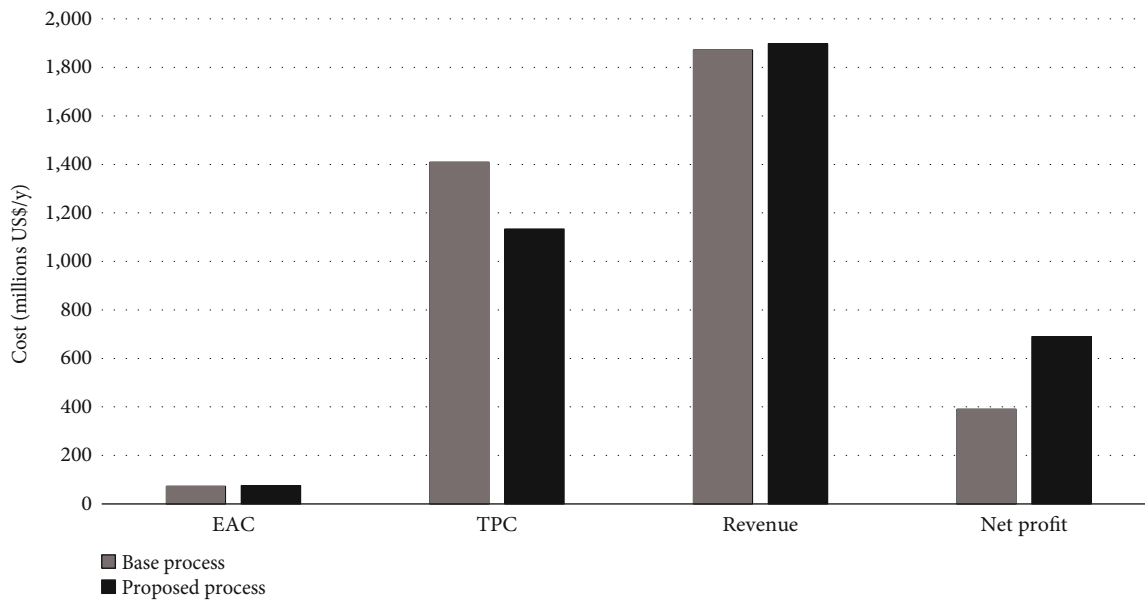
Figure 8: Comparison of the conventional and proposed systems with EAC, TPC, revenue, and net profit.

supply, water supply, waste disposal, and infrastructure construction [52]. C_{indirect} is the sum of engineering, construction, contractor, and contingency costs [53]. The expressions for calculating C_{direct} and C_{indirect} are shown in Equations (19) and (20), respectively.

$$C_{\text{direct}} = C_{\text{ISBL}} + C_{\text{OSBL}}, \tag{19}$$

$$C_{\text{indirect}} = C_{\text{contingency}} + C_{\text{contractor}} + C_{\text{engineering}} + C_{\text{construction}}. \tag{20}$$

Working capital investment (WCI) is the capital required to run a typical factory, such as the money needed to buy raw materials and provide electricity [54]. The start-up cost (SUC)

is the initial cost of starting a new design and is considered a one-time cost [55]. The expressions for the WCI and SUC are given in

$$\text{WCI} = 0.2 \times \text{FCI}, \tag{21}$$

$$\text{SUC} = 0.1 \times \text{FCI}. \tag{22}$$

The EAC can be calculated using the previous Equation (17), and the obtained values are summarized in Table 5.

3.2.2. Total Product Cost and Revenue. TPC represents the yearly expenses related to production, including labor, raw materials, and utilities. According to Equation (23), a 365-day operating period was used, with the direct production
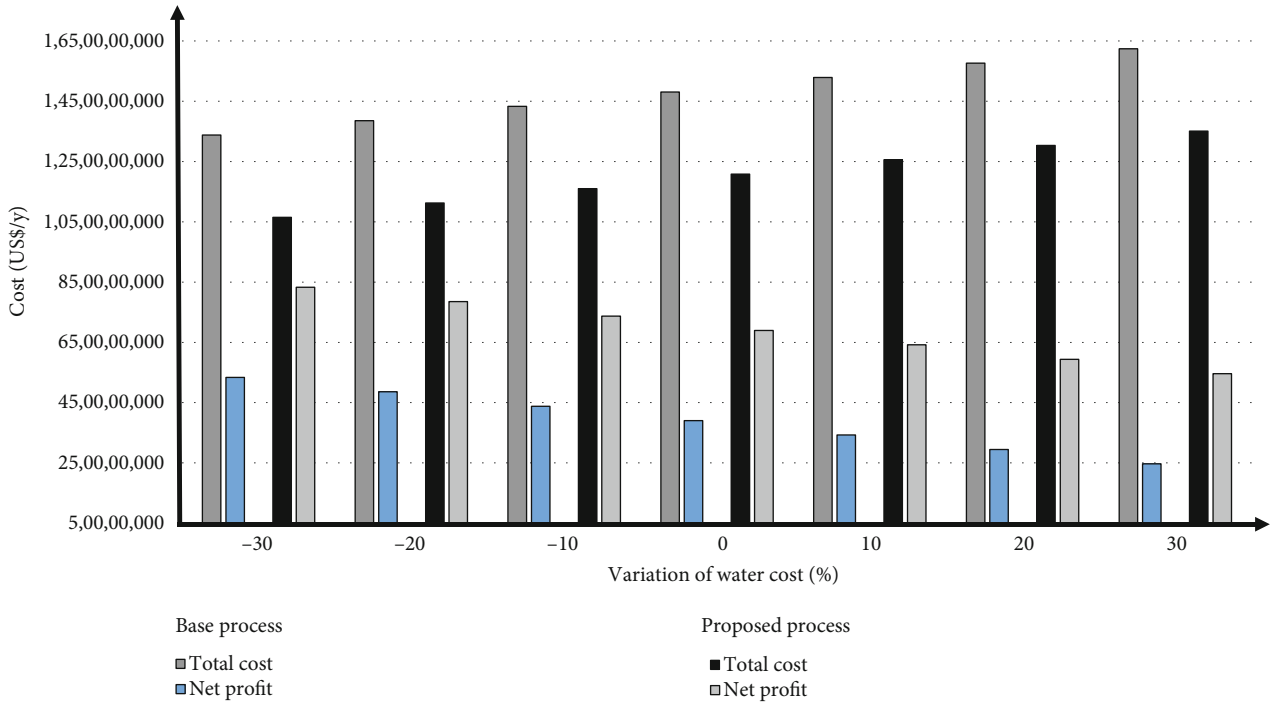
Figure 9: Overall cost and net profit of conventional and proposed systems according to variation in water costs.
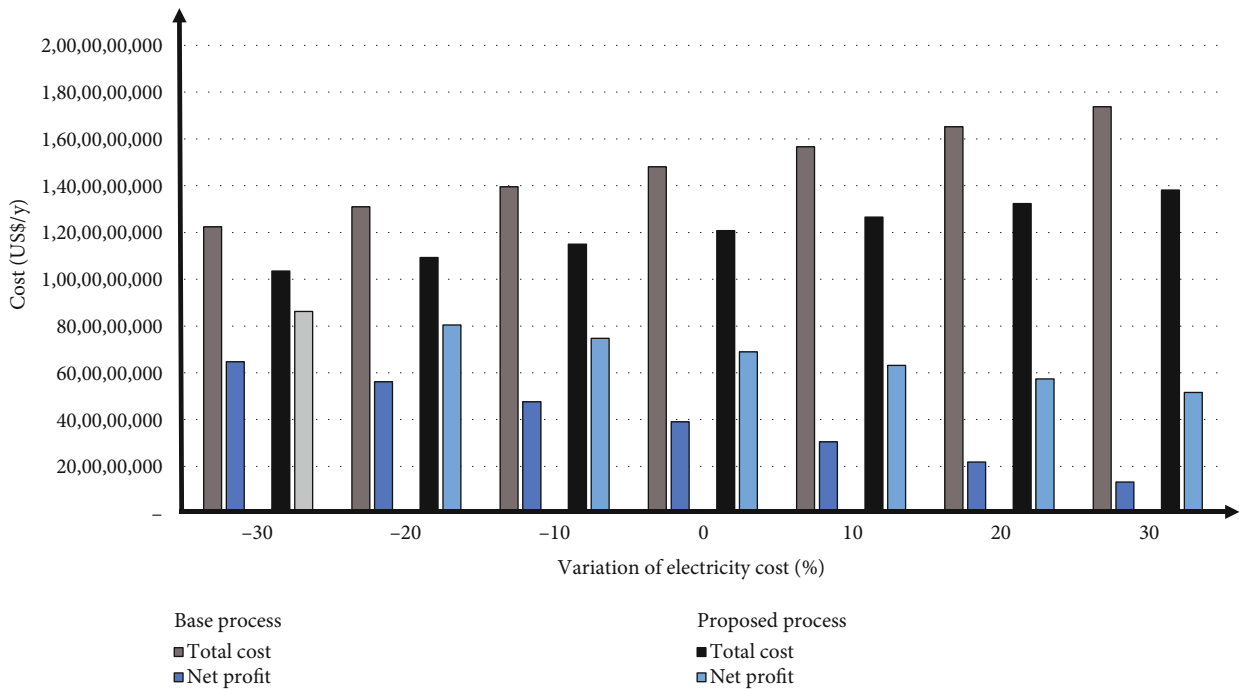
Figure 10: Overall cost and net profit of conventional and proposed systems according to variation in electricity costs.

cost (DPC) and general expense (GE) combined to calculate the total product cost (TPC) [60].

$$TPC = DPC + GE. \qquad (23)$$

DPC refers to direct costs such as raw materials, labor, and energy used to manufacture a product. GE are the indirect costs incurred by a business as it operates. These costs are not directly related to the production or sale of the
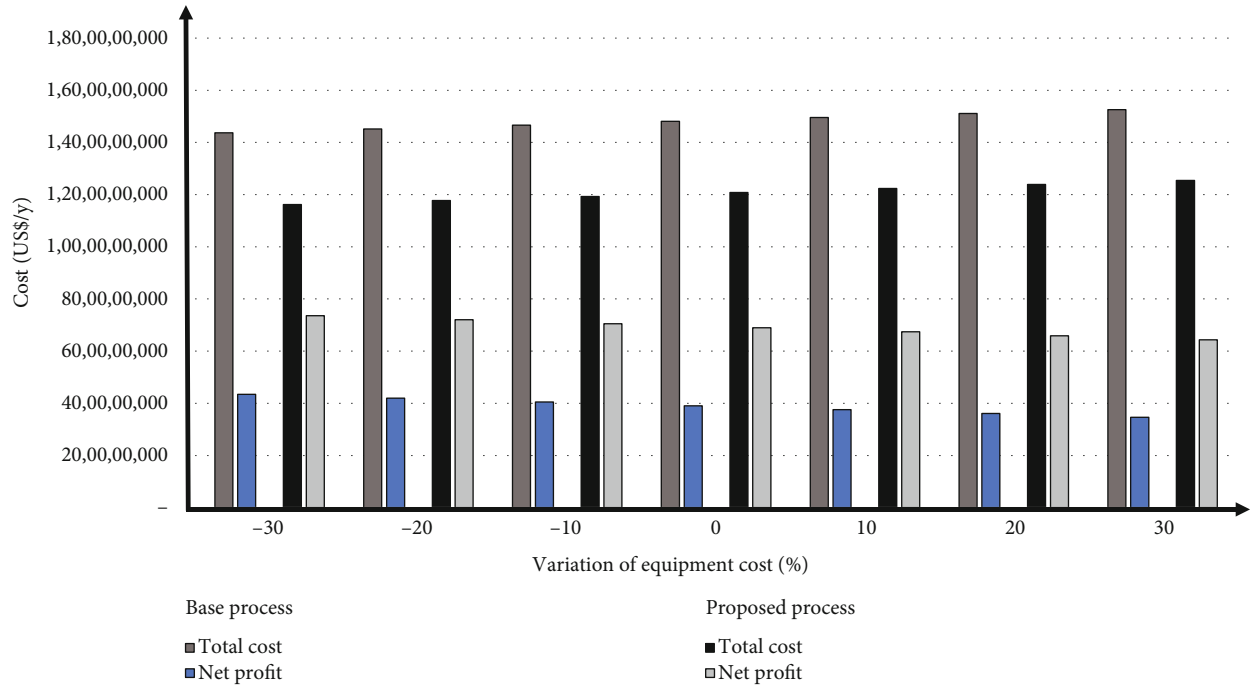
Figure 11: Overall cost and net profit of conventional and proposed systems according to variation in equipment costs.

Table 7: Heat and material balance of stream in the LNG vaporization process.

Stream name	AIR	BOG	BOG2	C-SEA-W2	LNG	LNG2	NG	SEA-W1
Temperature (°C)	20	-49.6	-140	5.8	-162	-159	10	15
Pressure (bar)	1	1.03	1.03	1	1	60	60	1
Mass flows (kg/s)	1264	0.008	0.008	639.3	31.71	31.72	31.7	639.3
Mass enthalpy (kJ/kg)	-5	-4718	-4912	-15943	-5429	-5417	-4658	-15905
Mass entropy (kJ/kg-K)	0.1341	-5.5709	-6.6907	-9.3272	-11.3530	-11.3775	-7.3136	-9.1952
Mole fractions								
CO_2	0	0	0	0	0	0	0	0
H_2O	0	0	0	1	0	0	0	1
O_2	0.21	0	0	0	0	0	0	0
N_2	0.79	0.0058	0.0058	0	0.00582	0.00582	5.82E-03	0
MEA	0	0	0	0	0	0	0	0
CH_4	0	0.9851	0.9851	0	0.98507	0.98507	9.85E-01	0
C_2H_6	0	0.0054	0.0054	0	0.00542	0.00542	5.42E-03	0
C_3H_8	0	0.0037	0.0037	0	0.00369	0.00369	3.69E-03	0
NH_3	0	0	0	0	0	0	0	0
Enthalpy flow (MW)	-6.695	-0.037	-0.039	-10193	-172	-172	-148	-10169

product. The DPC and GE are calculated using Equations (24) and (25), respectively [61].

$$DPC = C_{electricity} + C_{supervision} + C_{labor} + C_{laboratory}$$
$$+ C_{operating\ supplies} + C_{maintenance} + C_{water} + C_{raw\ materials}, \tag{24}$$

$$GEs = C_{R\&D} + C_{administrative} + C_{marketing}. \tag{25}$$

In addition, revenue is determined based on the electricity generated by the gas and steam turbines. Table 6 shows the TPC for both the conventional and proposed systems.

3.2.3. Economic Assessment Results. Figure 8 presents a comparison between the EAC, TPC, revenue, and net profit of the conventional and proposed systems. As shown in Figure 8, the EAC for the conventional and proposed systems is 72 and 75 million US$/y, respectively. The proposed

TABLE 8: Heat and material balance of stream in the NGCC process.

Stream name	FG	FG2	FG3	F-WATER	STEAM1	STEAM2	COND-W	SEA-W2	H-SEA-W	H-SEA-W2	W-SEA-W4
Temperature (°C)	2220	1243.9	183	60	767.2	137	60.4	15	77.5	67.7	61.5
Pressure (bar)	40	1.06	1.06	75	75	1	1	1	1	1	1
Mass flows (kg/s)	1295.7	1295.7	1295.7	439.5	439.5	439.5	439.5	4166.7	4166.7	4166.7	1027.8
Mass enthalpy (kJ/kg)	1456	130	-1154	-15718	-11932	-13215	-15716	-15905	-15642	-15684	-15711
Mass entropy (kJ/kg-K)	1.5782	1.9727	0.5471	-8.6152	-1.9558	-1.8642	-8.5874	-9.1952	-8.3721	-8.4950	-8.5734
Mole fractions											
CO_2	4.28E-02	4.28E-02	4.28E-02	0	0	0	0	0	0	0	0
H_2O	8.51E-02	8.51E-02	8.51E-02	1	1	1	1	1	1	1	1
O_2	1.16E-01	1.16E-01	1.16E-01	0	0	0	0	0	0	0	0
N_2	7.56E-01	7.56E-01	7.56E-01	0	0	0	0	0	0	0	0
MEA	0	0	0	0	0	0	0	0	0	0	0
CH_4	5.54E-19	5.54E-19	5.54E-19	0	0	0	0	0	0	0	0
C_2H_6	5.03E-35	5.03E-35	5.03E-35	0	0	0	0	0	0	0	0
C_3H_8	0	0	0	0	0	0	0	0	0	0	0
NH_3	1.31E-09	1.31E-09	1.31E-09	0	0	0	0	0	0	0	0
Enthalpy flow (MW)	1887	168	-1495	-6907	-5244	-5808	-6907	-66272	-65173	-65352	-16148

TABLE 9: Heat and material balance of stream in the amine scrubbing process.

Stream name	LOW2	CLEANGAS	CO2	C-SEA-W3	W-SEA-W1	DIST	FEEDGAS	LEAN1	LEAN2	MA-MEA	MA-WATER	MIXLEAN	MIXLEAN2	MIXLEAN3	RICH1	RICH2	RICH3
Temperature (°C)	67.4	65	35	5.8	35.1	92.5	182.2	100.9	35	38		45.6	45.6	37	72.5	73.3	80
Pressure (bar)	1.05	1	1	1	1	1	1.05	1.05	1	1		1	1.08	1.08	1.05	1.1	1.05
Mass flows (kg/s)	267.1	1208.0	87.6	115.1	115.1	207.5	1295.7	267.1	119.8	0.00035	0	386.9	386.9	386.9	474.5	474.5	474.5
Mass enthalpy (KJ/kg)	-15622	-721	-9016	-15943	-15823	-11467	-1155	-15474	-15985	-4376	-15815	-15734	-15734	-15770	-14315	-14314	-14231
Mass entropy (kJ/kg-K)	-8.4884	0.1949	0.0831	-9.3272	-8.9188	-0.9311	0.5479	-8.0792	-9.3271	-7.9701	-8.8931	-8.7716	-8.7716	-8.8851	-6.6018	-6.6014	-6.3614
Mole fractions																	
CO_2	3.60E-66	0.00013	0.95604	0	0	2.25E-01	4.28E-02	3.60E-66	6.38E-05	0	0	1.98E-05	1.98E-05	1.98E-05	8.33E-02	8.33E-02	8.33E-02
H_2O	9.98E-01	0.08705	0.04390	1	1	7.75E-01	8.51E-02	9.98E-01	1.00E+00	0	0	9.99E-01	9.99E-01	9.99E-01	9.16E-01	9.16E-01	9.16E-01
O_2	9.27E-70	0.12102	0.00001	0	0	3.30E-06	1.16E-01	9.27E-70	2.24E-11	0	0	6.97E-12	6.97E-12	6.97E-12	1.22E-06	1.22E-06	1.22E-06
N_2	6.59E-76	0.79180	0.00005	0	0	1.18E-05	7.56E-01	6.59E-76	3.04E-12	0	0	9.45E-13	9.45E-13	9.45E-13	4.36E-06	4.36E-06	4.36E-06
MEA	1.65E-03	0.00000	0.00000	0	0	6.60E-06	0	1.65E-03	7.84E-06	1	0	1.14E-03	1.14E-03	1.14E-03	1.04E-03	1.04E-03	1.04E-03
CH_4	0	0	0	0	0	0	5.54E-19	0	0	0	0	0	0	0	0	0	0
C_2H_6	0	0	0	0	0	0	5.03E-35	0	0	0	0	0	0	0	0	0	0
C_3H_8	0	0	0	0	0	0	0	0	0	0	0	0	0	0	0	0	0
NH_3	9.19E-29	0	2.94E-08	0	0	7.07E-09	1.31E-09	9.19E-29	2.09E-10	0	0	6.50E-11	6.50E-11	6.50E-11	2.62E-09	2.62E-09	2.62E-09
Enthalpy flow (MW)	-4172	-871	-790	-1835	-1821	-2379	-1496	-4133	-1915	-0.0015	0	-6088	-6088	-6101	-6793	-6793	-6753

Table 10: Heat and material balance of stream in the CO_2 liquefy process.

Stream name	C1	C2	C3	C4	C5	C6	C7	C8	C9	C10	C11	C12	C13	C14	C-SEA-W4	C-SEA-W5	W-SEA-W2	W-SEA-W3	LIQUID1
Temperature (°C)	373.2	35	35.0	35.0	206.6	35	35	-95.8			-95.8	-93.7	-22.69	5	5.8	5.8	37.1	36.8	35.0
Pressure (bar)	19.7	19.7	19.7	19.7	100	100	100	19.7			19	90	90	90	1	1	1	1	19.7
Mass flows (kg/s)	87.6	87.6	86.2	86.2	86.2	86.2	86.2	86.2			86.2	86.2	86.2	86.2	268.5	255.7	268.5	255.7	1.5
Mass enthalpy (kJ/kg)	-8677	-9072	-8955	-8955	-8814	-9193	-9193	-9193			-9193	-9186	-9331	-9296	-15943	-15943	-15814	-15816	-15820
Mass entropy (kJ/kg-K)	0.2404	-0.6453	-0.5020	-0.5020	-0.4168	-1.5096	-1.5096	-1.2637			-1.2635	-1.2639	-1.9845	-1.8565	-9.3272	-9.3272	-8.8918	-8.8960	-8.9255
Mole fractions																			
CO2	0.95604	0.95604	0.99634	0.99634	0.99634	0.99634	0.99634	0.99634	0	0	9.96E-01	9.96E-01	9.96E-01	9.96E-01	0	0	0	0	3.18E-06
H2O	0.04390	0.04390	0.00359	0.00359	0.00359	0.00359	0.00359	0.00359	0	0	3.59E-03	3.59E-03	3.59E-03	3.59E-03	1	1	1	1	1.00E+00
O2	0.00001	0.00001	0.00001	0.00001	0.00001	0.00001	0.00001	0.00001	0	0	1.46E-05	1.46E-05	1.46E-05	1.46E-05	0	0	0	0	3.49E-11
N2	0.00005	0.00005	0.00005	0.00005	0.00005	0.00005	0.00005	0.00005	0	0	5.21E-05	5.21E-05	5.21E-05	5.21E-05	0	0	0	0	1.93E-11
MEA	0.00000	0.00000	0.00000	0.00000	0.00000	0.00000	0.00000	0.00000	0	0	6.15E-09	6.15E-09	6.15E-09	6.15E-09	0	0	0	0	6.40E-05
CH4	0	0	0	0	0	0	0	0	0	0	0	0	0	0	0	0	0	0	0
C2H6	0	0	0	0	0	0	0	0	0	0	0	0	0	0	0	0	0	0	0
C3H8	0	0	0	0	0	0	0	0	0	0	0	0	0	0	0	0	0	0	0
NH3	2.94E-08	2.94E-08	3.02E-08	3.02E-08	3.02E-08	3.02E-08	3.02E-08	3.02E-08			3.02E-08	3.02E-08	3.02E-08	3.02E-08	0	0	0	0	9.16E-09
Enthalpy flow (MW)	-760	-795	-771	-771	-759	-792	-792	-792	—	—	-792	-791	-804	-801	-4281	-4077	-4246	-4044	-24

TABLE 11: Heat and material balance of stream in the CO_2 injection process.

Stream name	FEED1	FEED2	FEED3	FEED4	W-SEA-W6	W-SEA-W5	SEA-W3	SEA-W4	H-SEA-W3
Temperature (°C)	-19.7	-19.7	37.7	-19.8	12.5	34.6	15	15.1	67.7
Pressure (bar)	1.9	6.23	6.23	1.9	3	3	1	3	3
Mass flows (kg/s)	416.7	416.7	416.7	416.7	277.8	4166.7	277.8	277.8	4166.7
Mass enthalpy (kJ/kg)	-4059	-4088	-2685	-2795	-15916	-15824	-15905	-15905	-15684
Mass entropy (kJ/kg-K)	-11.4585	-11.5788	-6.6435	-6.4716	-9.2320	-8.9256	-9.1952	-9.1951	-8.4949
Mole fractions									
CO2	0	0	0	0	0	0	0	0	0
H2O	0	0	0	0	1	1	1	1	1
O2	0	0	0	0	0	0	0	0	0
N2	0	0	0	0	0	0	0	0	0
MEA	0	0	0	0	0	0	0	0	0
CH4	0	0	0	0	0	0	0	0	0
C2H6	0	0	0	0	0	0	0	0	0
C3H8	0	0	0	0	0	0	0	0	0
NH3	1	1	1	1	0	0	0	0	0
Enthalpy flow (MW)	-1691	-1703	-1119	-1165	-4421	-65935	-4418	-4418	-65351

system has a slightly higher EAC than conventional systems because it requires additional pumps, turbines, and heat exchangers. However, the TPC of the proposed system was approximately 20% less than that of the conventional system. This is attributed to the recovery of waste energy, resulting in a TPC of 1,133 million US$/y for the proposed system compared to 1,409 million US$/y for the conventional system. Finally, the net profit for the default and proposed systems was calculated to be 390.2 and 689.5 US$ million/y, respectively, demonstrating that the net profit for the proposed system increased by approximately 76.7%.

3.3. Sensitivity Analysis. The TAC of the proposed and conventional systems was derived by controlling EAC and TPC, and a sensitivity analysis was conducted to assess how the TAC obtained could change with variations in each variable. Specifically, the TAC of both systems was analyzed in response to variations in water, electricity, and equipment costs. Figure 9 illustrates the overall cost and net profit of the conventional and proposed systems based on the varying water costs.

The cost of water can vary depending on variables such as supply, demand, and overall production. From Figure 9, for −30, −20, −10, 10, 20, and 30% variations of water cost, the net profit for the conventional system was 534.6, 485.8, 438.0, 342.5, 294.7, and 246.9 million US$/y, respectively. Conversely, the net profit of the proposed system was 832.8, 785.1, 737.3, 641.7, 593.9, and 546.1 million US$/year, respectively, for a −30, −20, −10, 10, 20, and 30% variation of water cost. In both cases, as the water cost increased, the net profit decreased, and despite the variation in the water cost, the profit of the proposed system was higher than that of the conventional system. Figure 10 illustrates the overall cost and net profit of the conventional and proposed systems according to the variation in electricity costs.

Electricity costs may also vary depending on variables such as the fuel cost for power generation. From Figure 10, for the −30, −20, −10%, 10, 20, and 30% variations in electricity cost, the net profits for the conventional system were 257.2, 301.6, 345.9, 434.6, 478.9, and 523.3 million US$/y, respectively. Conversely, the net profit of the proposed system was 465.0, 539.8, 614.6, 764.3, 839.2, and 914.0 million US$/y, respectively, for a −30, −20, −10, 10, 20, and 30% variation of electricity costs. In both cases, the net profit also increases with increasing electricity costs. Unlike the fluctuation in the water cost, the difference between the net profits of the conventional and proposed systems gradually increased with an increase in the electricity cost. This is because the proposed system can generate more electricity and consume less electricity than a conventional system by applying an ORC. As a result, the net profit difference increases as the electricity cost increases; that is, the net profit difference between the proposed and conventional systems is 88% higher when the electricity cost increases by 30% (390.7 million US$/year) than when the electricity cost decreases by 30% (207.8 million US$/year). Finally, Figure 11 illustrates the overall cost and net profit of the conventional and proposed systems according to variations in the equipment cost.

From Figure 11, for −30, −20, −10, 10, 20, and 30% variations in electricity cost, the net profits for the conventional system were 434.4, 419.7, 405.0, 375.5, 360.8, and 346.1 million US$/y, respectively. Conversely, the net profit of the proposed system was 735.4, 720.1, 704.8, 674.2, 658.9, and 643.6 million US$/y, respectively, for a −30, −20, −10, 10, 20, and 30% variation of equipment costs. In both cases, as the electricity cost increased, the net profit decreased. Contrary to the trend of changes in net profit based on varying electricity costs, the difference in net profit between the conventional and proposed systems decreased as the equipment cost increased. This is because the increased

equipment cost due to the installation of additional devices in the proposed system has a greater impact. However, despite the change in equipment costs resulting from the increased number of devices in the proposed system, the net profit of the proposed system was higher than that of the conventional system in all cases. This implies that the benefits of installing additional devices outweigh the associated installation costs.

4. Conclusion

This study contributes to the existing knowledge by introducing a newly developed waste heat and cold energy recovery system for a post-combustion LNG power plant using an ORC. The system aims to recover waste heat and cold energy by utilizing the temperature difference as a driving force to generate power. This study makes contributes to the existing literature in two significant ways:

(i) Recovery of waste cooling energy: The system effectively recovers waste cooling energy from the LNG vaporization process and utilizes it to cool the LEAN solution and liquefy CO_2. This approach maximizes energy efficiency by effectively using the available waste energy

(ii) Novel configuration of the CO_2 injection part: The system incorporates a unique configuration for the CO_2 injection part using the ORC. This configuration increases the efficiency of waste heat recovery from the NGCC to pressurize and heat the liquefied CO_2, resulting in a lower specific net power consumption and higher power efficiency

The results of the study indicate that the proposed system can achieve a significant increase of 18.6% in net power generation compared to the conventional system. In addition, the net profit of the proposed system can be enhanced by 76.7% compared to that of the conventional system, demonstrating its high economic feasibility. In addition, in order to mitigate greenhouse gas CO_2 emissions, a substantial amount of steam and cold energy is employed. However, the generation of this energy may result in additional CO_2 emissions. Consequently, this study proposes that the energy required for CCS can be significantly diminished through the recovery of waste heat, thereby maximizing the reduction of CO_2 emissions. Therefore, the proposed system offers significant economic and environmental benefits. This work focused on the conceptual design of waste energy recovery system for LNG power plant using ORC. However, in the proposed system, parameters such as absorbing type of CCS or working fluid and temperature of ORC were not optimally considered. In addition, despite the utilization of a two-phase ORC, it is essential to conduct an efficiency comparison across a spectrum of Rankine cycles, including the simple ORC, regenerative ORC, cascade ORC, organic flash cycle, alternative Rankine configurations, and the trilateral cycle. Therefore, in the further studies, it is crucial to consider and optimize system parameters to enhance field applicability and maximize cost-effectiveness.

Appendix

A. Heat and Material Balance

The heat and material balance of key streams as the simulation results are listed in Tables 7, 8, 9, 10, and 11.

Nomenclature

AF:	Annuity factor
BOG:	Boil-off gas
CCS:	CO_2 capture and storage
COM (1-2):	Compressor
COND (1-3):	Condenser
C_{direct}:	Direct cost (US$)
$C_{indirect}$:	Indirect cost (US$)
C_{ISBL}:	Inside battery limit cost (US$)
C_{OSBL}:	Outside battery limit cost (US$)
$C_{contingency}$:	Contingency cost (US$)
$C_{contractor}$:	Contractor cost (US$)
$C_{engineering}$:	Engineering cost (US$)
$C_{construction}$:	Construction cost (US$)
$C_{electricity}$:	Electricity cost (US$)
$C_{supervision}$:	Supervision cost (US$)
C_{labor}:	Labor cost (US$)
$C_{laboratory}$:	Laboratory cost (US$)
$C_{operating\ supplies}$:	Operating supply cost (US$)
$C_{maintenance}$:	Maintenance cost (US$)
C_{water}:	Water cost (US$)
$C_{raw\ materials}$:	Raw material cost (US$)
$C_{administrative}$:	Administrative cost (US$)
$C_{marketing}$:	Marketing cost (US$)
$C_{R\&D}$:	R&D cost (US$)
DPC:	Direct production cost (US$)
EAC:	Equivalent annual cost (US$)
FCI:	Fixed capital investment (US$)
GE:	General expense (US$)
G-TUR:	Gas turbine
HRSG:	Heat recovery steam generator
H-EX(1-9):	Heat exchanger
HP-TUR:	High-pressure steam turbine
LNG:	Liquefied natural gas
LP-TUR:	Low-pressure steam turbine
n:	Number of periods
NGCC:	Natural gas combined cycle
ORC:	Organic Rankine cycle
r:	Interest rate
SUC:	Start-up cost (US$)
SEA-W(1-3):	Seawater
ORC-TUR:	ORC turbine
STR-R:	Stripper reboiler
STR-C:	Stripper condenser
TPC:	Total product cost (US$)
TCI:	Total capital cost (US$)
WCI:	Working capital investment (US$).

Data Availability

The data used to support the findings of this study are available from the corresponding authors upon request.

Conflicts of Interest

The authors declare that they have no known competing financial interests or personal relationships that could have influenced the work reported in this paper.

Authors' Contributions

Minsik Choi and Jonghun Lim contributed equally to this work and are co-first authors.

Acknowledgments

References

[1] F. Kong, G. Rim, M. Song et al., "Research needs targeting direct air capture of carbon dioxide: material & process performance characteristics under realistic environmental conditions," *Korean Journal of Chemical Engineering*, vol. 39, no. 1, pp. 1–19, 2022.

[2] J. Park, H. Mun, J. Kim, and I. Lee, "Advanced natural gas liquefaction process on LNG supply chain with liquid air: from design to thermodynamic and techno-economic analyses," *Energy Conversion and Management*, vol. 252, article 115107, 2022.

[3] A. R. Kalair, M. Seyedmahmoudian, A. Stojcevski, N. Abas, and N. Khan, "Waste to energy conversion for a sustainable future," *Heliyon*, vol. 7, no. 10, article e08155, 2021.

[4] K. Chen, H. Yu, G. Fan, Y. Zhang, and Y. Dai, "Multi-objective optimization of a novel combined parallel power generation system using CO_2 and N_2 for cascade recovery of LNG cryogenic energy," *Energy Conversion and Management*, vol. 256, article 115395, 2022.

[5] M. J. Chae, J. H. Kim, B. Moon, S. Park, and Y. S. Lee, "The present condition and outlook for hydrogen-natural gas blending technology," *Korean Journal of Chemical Engineering*, vol. 39, no. 2, pp. 251–262, 2022.

[6] S. Z. S. Al Ghafri, C. Revell, M. Di Lorenzo et al., "Techno-economic and environmental assessment of LNG export for hydrogen production," *International Journal of Hydrogen Energy*, vol. 48, no. 23, pp. 8343–8369, 2023.

[7] J. Park, F. You, H. Mun, and I. Lee, "Liquefied natural gas supply chain using liquid air as a cold carrier: novel method for energy recovery," *Energy Conversion and Management*, vol. 227, article 113611, 2021.

[8] M.-K. Kim, G. Han, H. Kim et al., "Optimization of water-saturated superabsorbent polymers for hydrate-based gas storage," *Korean Journal of Chemical Engineering*, vol. 40, no. 5, pp. 1063–1070, 2023.

[9] H. Sultan, H. A. Muhammad, U. H. Bhatti et al., "Reducing the efficiency penalty of carbon dioxide capture and compression process in a natural gas combined cycle power plant by process modification and liquefied natural gas cold energy integration," *Energy Conversion and Management*, vol. 244, article 114495, 2021.

[10] W. Qiang, L. Yanzhong, and C. Xi, "Exergy analysis of liquefied natural gas cold energy recovering cycles," *International Journal of Energy Research*, vol. 29, no. 1, pp. 65–78, 2005.

[11] I. Lee, J. Park, F. You, and I. Moon, "A novel cryogenic energy storage system with LNG direct expansion regasification: design, energy optimization, and exergy analysis," *Energy*, vol. 173, pp. 691–705, 2019.

[12] A. Paudel and T. Bandhauer, "Techno-economic analysis of waste heat recovery systems for wet-cooled combined cycle power plants," *Applied Thermal Engineering*, vol. 143, pp. 746–758, 2018.

[13] S. Cho, J. Park, W. Noh, I. Lee, and I. Moon, "Developed hydrogen liquefaction process using liquefied natural gas cold energy: design, energy optimization, and techno-economic feasibility," *International Journal of Energy Research*, vol. 45, no. 10, pp. 14745–14760, 2021.

[14] J. Lim, Y. Kim, H. Cho, J. Lee, and J. Kim, "Novel process design for waste energy recovery of LNG power plants for CO_2 capture and storage," *Energy Conversion and Management*, vol. 277, p. 116587, 2023.

[15] J. Lim, J. Lee, I. Moon, H. Cho, and J. Kim, "Techno-economic comparison of amine regeneration process with heat-stable amine salt reclaiming units," *Energy Science and Engineering*, vol. 9, no. 12, pp. 2529–2543, 2021.

[16] H. You, Y. Seo, C. Huh, and D. Chang, "Performance analysis of cold energy recovery from CO_2 injection in ship-based carbon capture and storage (CCS)," *Energies*, vol. 7, no. 11, pp. 7266–7281, 2014.

[17] C.-C. Cormos, "Assessment of chemical absorption/adsorption for post-combustion CO_2 capture from natural gas combined cycle (NGCC) power plants," *Applied Thermal Engineering*, vol. 82, pp. 120–128, 2015.

[18] X. Ye, Z. Dong, J. Lu, and C. Li, "Thermoeconomic evaluation of double-reheat coal-fired power units with carbon capture and storage and waste heat recovery using organic Rankine cycle," *International Journal of Greenhouse Gas Control*, vol. 105, article 103247, 2021.

[19] Z. Zhang, D.-N. Vo, J. Kum, S.-H. Hong, and C.-H. Lee, "Enhancing energy efficiency of chemical absorption-based CO_2 capture process with advanced waste-heat recovery modules at a high capture rate," *Chemical Engineering Journal*, vol. 472, article 144918, 2023.

[20] Y. Hu, L. Zhang, H. Lv, S. Lu, G. Xu, and C. Xu, "A low energy consumption de-carbonization natural gas combined cycle power generation system based on $LiBr/H_2O$ absorption heat transformer," *International Journal of Greenhouse Gas Control*, vol. 109, article 103389, 2021.

[21] R. K. Garlapalli, M. W. Spencer, K. Alam, and J. P. Trembly, "Integration of heat recovery unit in coal fired power plants to reduce energy cost of carbon dioxide capture," *Applied Energy*, vol. 229, pp. 900–909, 2018.

[22] P. Talebizadehsardari, M. A. Ehyaei, A. Ahmadi et al., "Energy, exergy, economic, exergoeconomic, and exergoenvironmental (5E) analyses of a triple cycle with carbon capture," *Journal of CO2 Utilization*, vol. 41, article 101258, 2020.

[23] H. Mun, H. Kim, J. Park, and I. Lee, "A novel boil-off gas reliquefaction system using liquid air for intercontinental liquefied natural gas transportation," *Energy Conversion and Management*, vol. 269, article 116078, 2022.

[24] S. Daniarta and A. R. Imre, "Cold energy utilization in LNG regasification system using organic Rankine cycle and trilateral flash cycle," *Periodica Polytechnica Mechanical Engineering*, vol. 64, no. 4, pp. 342–349, 2020.

[25] J. Bao, T. Yuan, L. Zhang, N. Zhang, X. Zhang, and G. He, "Comparative study of liquefied natural gas (LNG) cold energy power generation systems in series and parallel," *Energy Conversion and Management*, vol. 184, pp. 107–126, 2019.

[26] P. K. Nag and S. De, "Design and operation of a heat recovery steam generator with minimum irreversibility," *Applied Thermal Engineering*, vol. 17, no. 4, pp. 385–391, 1997.

[27] I. H. Aljundi, "Energy and exergy analysis of a steam power plant in Jordan," *Applied Thermal Engineering*, vol. 29, no. 2-3, pp. 324–328, 2009.

[28] T. He and W. Lin, "Energy saving research of natural gas liquefaction plant based on waste heat utilization of gas turbine exhaust," *Energy Conversion and Management*, vol. 225, article 113468, 2020.

[29] J. Xu and W. Lin, "A CO_2 cryogenic capture system for flue gas of an LNG-fired power plant," *International Journal of Hydrogen Energy*, vol. 42, no. 29, pp. 18674–18680, 2017.

[30] M. R. Gómez, R. F. Garcia, J. R. Gómez, and J. C. Carril, "Thermodynamic analysis of a Brayton cycle and Rankine cycle arranged in series exploiting the cold exergy of LNG (liquefied natural gas)," *Energy*, vol. 66, pp. 927–937, 2014.

[31] J. Lim, S. Jeong, and J. Kim, "Deep neural network-based optimal selection and blending ratio of waste seashells as an alternative to high-grade limestone depletion for SOX capture and utilization," *Chemical Engineering Journal*, vol. 431, article 133244, 2022.

[32] Y. Seo, C. Huh, and D. Chang, "Economic evaluation of CO_2 liquefaction processes for ship-based carbon capture and storage (CCS) chain," in *The Twenty-Fourth International Ocean and Polar Engineering Conference*, Busan, Korea, June 2014.

[33] W. Zhang, C. Sun, C. E. Snape et al., "Process simulations of post-combustion CO_2 capture for coal and natural gas-fired power plants using a polyethyleneimine/silica adsorbent," *International Journal of Greenhouse Gas Control*, vol. 58, pp. 276–289, 2017.

[34] H. K. Kayadelen, "Effect of natural gas components on its flame temperature, equilibrium combustion products and thermodynamic properties," *Journal of Natural Gas Science and Engineering*, vol. 45, pp. 456–473, 2017.

[35] J. Bobek, D. Rippel-Pethő, É. Molnár, and R. Bocsi, "Selective hydrogen sulphide removal from acid gas by alkali chemisorption in a jet reactor," *Hungarian Journal of Industry and Chemistry*, vol. 44, no. 1, pp. 51–54, 2016.

[36] M. A. Darwish and A. B. Amer, "Cost allocation in cogeneration power-desalination plant utilising gas/steam combined cycle (GTCC) in Kuwait," *International Journal of Exergy*, vol. 14, no. 3, p. 275, 2014.

[37] Energy Agency I, "Technology perspectives energy special report on carbon capture utilisation and storage CCUS in clean energy transitions," *Energy Technology Perspectives*, vol. 2020, 2020.

[38] S. Lee, "Multi-parameter optimization of cold energy recovery in cascade Rankine cycle for LNG regasification using genetic algorithm," *Energy*, vol. 118, pp. 776–782, 2017.

[39] P. Khakharia, J. Mertens, T. J. H. Vlugt, and E. Goetheer, "Predicting aerosol based emissions in a post combustion CO_2 capture process using an Aspen plus model," *Energy Procedia*, vol. 63, pp. 911–925, 2014.

[40] Y. Seo, H. You, S. Lee, C. Huh, and D. Chang, "Evaluation of CO_2 liquefaction processes for ship-based carbon capture and storage (CCS) in terms of life cycle cost (LCC) considering availability," *International Journal of Greenhouse Gas Control*, vol. 35, pp. 1–12, 2015.

[41] E. Latosov, M. Loorits, B. Maaten, A. Volkova, and S. Soosaar, "Corrosive effects of H_2S and NH_3 on natural gas piping systems manufactured of carbon steel," *Energy Procedia*, vol. 128, pp. 316–323, 2017.

[42] S. Daniarta, P. Kolasiński, and A. R. Imre, "Thermodynamic efficiency of trilateral flash cycle, organic Rankine cycle and partially evaporated organic Rankine cycle," *Energy Conversion and Management*, vol. 249, article 114731, 2021.

[43] J. Ding, B. Freeman, and G. T. Rochelle, "Regeneration design for NGCC CO_2 capture with amine-only and hybrid amine/membrane," *Energy Procedia*, vol. 114, pp. 1394–1408, 2017.

[44] H. Ahn, M. Luberti, Z. Liu, and S. Brandani, "Process configuration studies of the amine capture process for coal-fired power plants," *International Journal of Greenhouse Gas Control*, vol. 16, pp. 29–40, 2013.

[45] L. Duan, M. Zhao, and Y. Yang, "Integration and optimization study on the coal-fired power plant with CO_2 capture using MEA," *Energy*, vol. 45, no. 1, pp. 107–116, 2012.

[46] J. Jung, Y. S. Jeong, U. Lee, Y. Lim, and C. Han, "New configuration of the CO_2 capture process using aqueous monoethanolamine for coal-fired power plants," *Industrial and Engineering Chemistry Research*, vol. 54, no. 15, pp. 3865–3878, 2015.

[47] J. Lim, H. Lee, H. Cho, J. Y. Shim, H. Lee, and J. Kim, "Novel waste heat and oil recovery system in the finishing treatment of the textile process for cleaner production with economic improvement," *International Journal of Energy Research*, vol. 46, no. 14, pp. 20480–20493, 2022.

[48] J. Lim and J. Kim, "Optimizing ash deposit removal system to maximize biomass recycling as renewable energy for CO_2 reduction," *Renewable Energy*, vol. 190, pp. 1006–1017, 2022.

[49] Y. Kim, J. Lim, J. Y. Shim, S. Hong, H. Lee, and H. Cho, "Optimization of heat exchanger network via pinch analysis in heat pump-assisted textile industry wastewater heat recovery system," *Energies*, vol. 15, no. 9, p. 3090, 2022.

[50] J. Lim, Y. Ahn, H. Cho, and J. Kim, "Optimal strategy to sort plastic waste considering economic feasibility to increase recycling efficiency," *Process Safety and Environmental Protection*, vol. 165, pp. 420–430, 2022.

[51] J. Lim, D. J. Kim, H. Cho, and J. Kim, "Design of novel seawater bittern recovery process for CO_2 and SO_x utilization," *Desalination*, vol. 540, article 115995, 2022.

[52] H. Lee, J. Lim, H. Cho, and J. Kim, "Novel pulp mill wastewater recovery process for CO_2 and SO_x utilization," *Journal of Cleaner Production*, vol. 371, article 133298, 2022.

[53] J. Lim and J. Kim, "Designing and integrating NO_x, SO_2 and CO_2 capture and utilization process using desalination wastewater," *Fuel*, vol. 327, article 124986, 2022.

[54] Y. Kim, J. Lim, H. Cho, and J. Kim, "Novel mechanical vapor recompression-assisted evaporation process for improving energy efficiency in pulp and paper industry," *International Journal of Energy Research*, vol. 46, no. 3, pp. 3409–3427, 2022.

[55] J. Lim, H. Cho, and J. Kim, "Optimization of wet flue gas desulfurization system using recycled waste oyster shell as high-grade limestone substitutes," *Journal of Cleaner Production*, vol. 318, article 128492, 2021.

[56] J. Lim, J. Lee, H. Cho, and J. Kim, "Model development of amine regeneration process with electrodialysis reclamation unit," in *31 European Symposium on Computer Aided Process Engineering*, M. Türkay and Gani RBT-CACE, Eds., vol. 50, pp. 579–584, Elsevier, 2021.

[57] L. Khani, S. M. S. Mahmoudi, A. Chitsaz, and M. A. Rosen, "Energy and exergoeconomic evaluation of a new power/cooling cogeneration system based on a solid oxide fuel cell," *Energy*, vol. 94, pp. 64–77, 2016.

[58] M. H. Ahmadi, M. Mehrpooya, and F. Pourfayaz, "Exergoeconomic analysis and multi objective optimization of performance of a carbon dioxide power cycle driven by geothermal energy with liquefied natural gas as its heat sink," *Energy Conversion and Management*, vol. 119, pp. 422–434, 2016.

[59] O. K. Singh and S. C. Kaushik, "Thermoeconomic evaluation and optimization of a Brayton–Rankine–Kalina combined triple power cycle," *Energy Conversion and Management*, vol. 71, pp. 32–42, 2013.

[60] Y. S. Jeong, J. Jung, U. Lee, C. Yang, and C. Han, "Techno-economic analysis of mechanical vapor recompression for process integration of post-combustion CO_2 capture with downstream compression," *Chemical Engineering Research and Design*, vol. 104, pp. 247–255, 2015.

[61] J. Lim, H. Cho, H. Kwon, H. Park, and J. Kim, "Reinforcement learning-based optimal operation of ash deposit removal system to improve recycling efficiency of biomass for CO_2 reduction," *Journal of Cleaner Production*, vol. 370, article 133605, 2022.

[62] Y. Kim, J. Lim, J. Y. Shim, H. Lee, H. Cho, and J. Kim, "Optimizing wastewater heat recovery systems in textile dyeing processes using pinch analysis," *Applied Thermal Engineering*, vol. 214, article 118880, 2022.